

3D-scanning microscopy with adaptive lenses and prisms for zebrafish studies

Wenjie Wang,^a Florian Lemke^{✉,b}, Matthias C. Wapler,^b Ulrike Wallrabe,^b
Jürgen W. Czarske,^{a,c,d} and Nektarios Koukourakis^{a,d,*}

^aTU Dresden, Laboratory for Measurement and Sensor System Techniques, Dresden, Germany

^bUniversity of Freiburg, Department of Microsystems Engineering-IMTEK, Laboratory for Microactuators, Freiburg, Germany

^cTU Dresden, Cluster of Excellence Physics of Life, Dresden, Germany

^dTU Dresden, Competence Center for Biomedical Computational Laser Systems, Dresden, Germany

Abstract. Point-scanning-based microscopy systems require combination of axial and lateral scanning to obtain three-dimensional (3D) data. Axial scanning was commonly achieved by mechanical displacement of the objective or the sample. To improve, various adaptive lens-based solutions have been reported to circumvent the need for mechanically moving parts. The lateral scanning is predominantly implemented using galvanometric mirrors. Although the performance of such devices is flawless, they require bulky, folded beam-paths that make their incorporation in compact hand-held devices challenging. Recently, we introduced an adaptive prism as a transmissive device that enables lateral scanning. We demonstrate the first all-adaptive 3D scanning in laser scanning microscopes employing a compact in-line transmission geometry without mechanically moving parts and beam folding, combining an adaptive lens and a novel adaptive prism. Characterization of the all-adaptive microscope performance shows a lateral tuning range of approximately $X = Y = 130 \mu\text{m}$ and an axial tuning range of about $Z = 500 \mu\text{m}$. We successfully demonstrate 3D raster scanning of the fluorescence of a thyroid of a zebrafish embryo. © The Authors. Published by SPIE under a Creative Commons Attribution 4.0 Unported License. Distribution or reproduction of this work in whole or in part requires full attribution of the original publication, including its DOI. [DOI: [10.1117/1.JOM.1.2.024501](https://doi.org/10.1117/1.JOM.1.2.024501)]

Keywords: 3D scanning; adaptive prism; adaptive lens; biomedical imaging.

Paper 21001 received Jan. 14, 2021; accepted for publication Mar. 19, 2021; published online Apr. 10, 2021.

1 Introduction

Adaptive optics technology has been employed in various systems to improve imaging properties,¹ correct aberrations,² and perform self-calibration.³ Imaging techniques that acquire information in a point-wise manner, such as confocal microscopy^{4,5} or optical coherence microscopy,^{6,7} require point-scanning in three dimensions to obtain three-dimensional (3D) data. One possible way to accomplish the axial scanning is to mechanically translate the sample^{8,9} or the microscope objective¹⁰ in z -direction.

Several approaches employing adaptive lenses^{11,12} have been introduced to realize axial scanning without the need for any mechanically moving parts in a variety of microscopes, such as confocal microscopy,^{2,13} two-photon microscopy,^{14,15} light-sheet microscopy,^{16–18} structured illumination microscopy,^{19,20} and standard wide-field microscopy.^{21,22} More sophisticated adaptive lenses with 2 degrees of freedom enabled simultaneously tuning the focal position and correcting the spherical aberrations. This lens is committed to correct for specimen-induced spherical aberrations that occur in deep tissue applications² and systematic scan-induced aberrations.¹²

*Address all correspondence to Nektarios Koukourakis, nektarios.koukourakis@tu-dresden.de

The lateral scan is accomplished by mechanical translation of the sample or by reflective galvanometric mirrors.²³ The direction of the reflected beam can be regulated by turning the mirror. This type of scanner has a high resolution, good repeatability, and low drift values. It can approach both static and dynamic angles and can be operated at comparatively high speeds. However, galvanometer mirrors in reflective systems require a folded beam path, thus resulting in bulky optical setups. Adaptive prisms have the potential to improve and to allow for lateral scanning within an in-line compact setup. The first adaptive prisms reported were based on electrowetting on dielectric.^{24–26} However, the scanning angle range of electrowetting-based prisms is too narrow to achieve a large field of view. Recently, we introduced a piezo-actuated adaptive prism with a large tuning range^{27,28} as a suitable alternative to galvanometer mirror that enables an in-line transmissive configuration with large scanning angle range.

In this paper, we combine the adaptive prism with an adaptive lens, to realize the first all-adaptive 3D scanning in an in-line transmission geometry. To demonstrate the ability for biomedical 3D imaging of our approach, we conduct raster scanning of the thyroid of a cultured zebrafish embryo.

2 Working Principles and Characteristics of Adaptive Elements

2.1 Adaptive Lens

The adaptive lens used in our all-adaptive scanning microscope consists of a transparent polydimethylsiloxan membrane, which is embedded in an annular piezo-bending actuator. Between the membrane and a glass substrate, an incompressible, transparent fluid is filled. When actuated, the bending actuator displaces the fluid underneath which generates a pressure inside the lens and deflects the membrane. We use a bimorph actuator (two piezo layers with opposite polarization) that provides large deflections in both directions. Such lenses have already been used in Refs. 13 and 19.

As the numerical aperture (NA) of the adaptive lens is small (maximum 0.2), it has to be used in conjunction with an objective lens with high NA. The adaptive lens is imaged close to the objective back aperture as this is the best compromise between a reduction of systematic aberrations and the axial tuning range of the system.²⁹ The working principle of adaptive lens is illustrated in Fig. 1(a).

2.2 Adaptive Prism

In Fig. 1(b), the working principle of adaptive prism is illustrated. The adaptive prism consists of a fixed glass substrate and a tiltable glass window that sandwich a fluid. The upper glass of the adaptive prism can be tilted by three piezo-bimorph bending transducers (see Fig. 2). As the wavefront tilt is induced by the adjustment of the controlled path-length caused by the refractive index transition from the fluid in the prism to air (approximately 1.48 to 1), a surface tilt of 1 deg is required to induce a wavefront tilt of 0.48 deg. It has been verified that the prism is capable to induce wavefront tilts up to ± 6.4 deg and achieves response times of 2.5 ms.²⁷

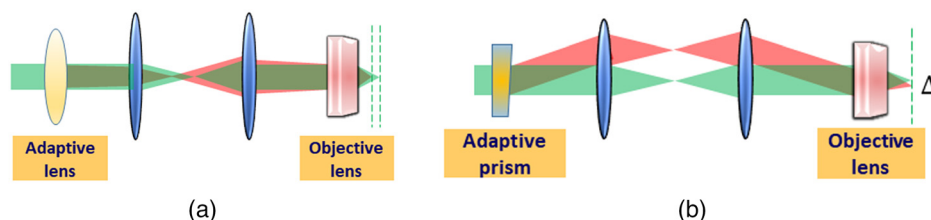


Fig. 1 (a) Schematic of the axial scanning setup with an adaptive lens. (b) Schematic of the lateral scanning setup using an adaptive prism.

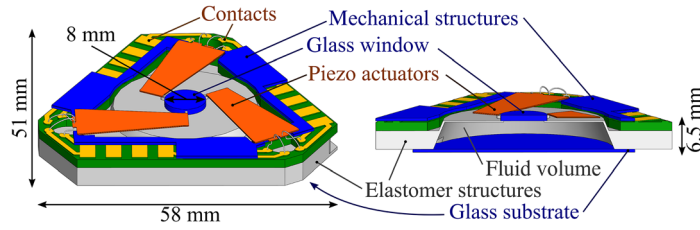


Fig. 2 Schematic of the adaptive prism.

3 Characterization of All-Adaptive 3D Scanning Microscope

3.1 Digital Holography for Characterization of Adaptive Components

The characterization of the individual adaptive lens and prism is performed using digital off-axis holography.³⁰

The adaptive element is illuminated (green beam) and the transmitted light is imaged onto the camera. There it is overlapped with a coherent plane wave, which acts as a reference beam (marked in red) Fig. 3. The change of the wavefront angle upon actuation is measured holographically. The reconstructed results are summarized in Fig. 4. The tuning range of the adaptive lens is in the range of -23 to 19 dpt. We show the wavefront tilt angle of the adaptive prism amounts to a scanning range of 12.8 deg. As the mounting of the adaptive prism is not perfectly aligned, tilting in the x -axis also leads to a small tilt in the y -axis direction.

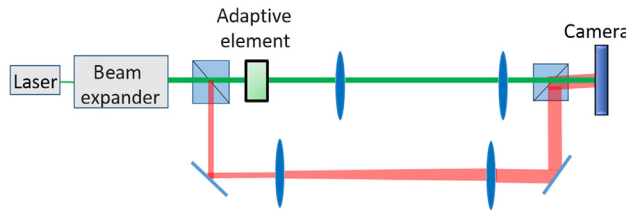


Fig. 3 Digital holographic setup in off-axis geometry for the characterization of the adaptive elements.

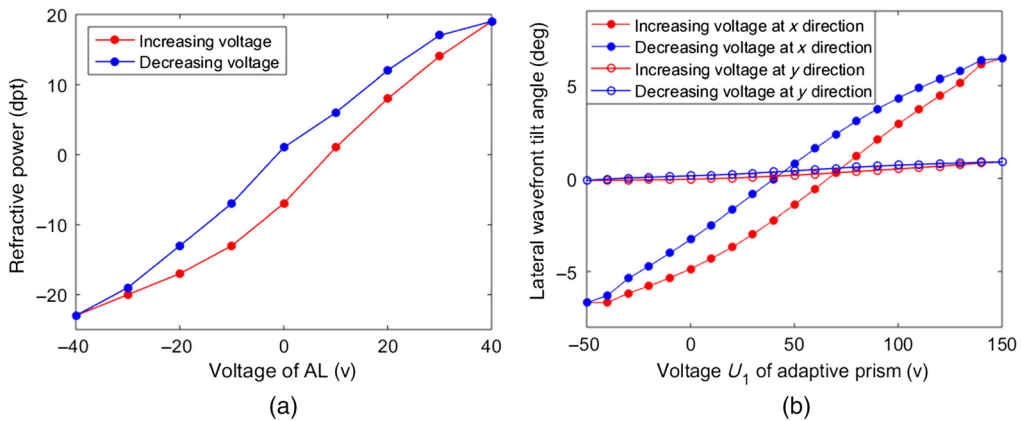


Fig. 4 (a) The refractive power of the adaptive lens as a function of the applied voltage U . (b) The lateral scanning angle of the adaptive prism as a function of voltage U_1 applied to adaptive prism. Also the induced undesired tilt across the perpendicular axis is displayed.

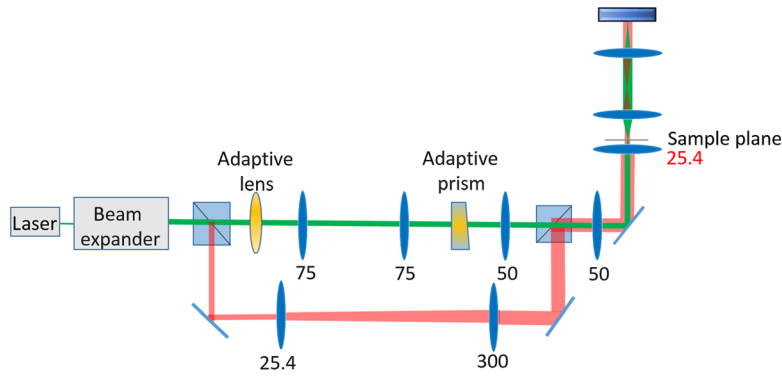


Fig. 5 The sketched digital holographic setup is used to characterize the scanning system. The green beam acts as an object beam, while the red beam is the reference beam. Actuation of the adaptive elements results in a shifting focus, which acts as a point-source.

3.2 Digital Holography for Characterization of the 3D Scanning

The characterization of the 3D scanning is performed with the in-line digital holographic system shown in Fig. 5. The laser beam (TCLDM9) at an output wavelength of 532 nm is expanded by a beam expander and illuminates the adaptive lens. A $4f$ imaging system consisting of two lenses with focal length of both 75 mm images the adaptive lens to the adaptive prism, which is again imaged to the front lens by two 50-mm lenses. In the first characterization measurements, the scanning lens has a focal length of 25.4 mm.

A reference beam marked in red is split, magnified, and is overlapped on the digital camera with the object beam. The object beam is the scanned focus, which acts as a point source. The region of interest is imaged to the camera together with the reference beam. The resulting interference rings allow to reconstruct the origin of the point source in 3D by digital propagation, employing the angular spectrum propagation.³⁰ The setup is designed in in-line geometry, which is sufficient to reconstruct the amplitude information of the scanned region. Hence, we can track the scanning of the focus position numerically and can characterize the system.

The all-adaptive 3D scanning system is driven as shown in Fig. 6. In these experiments, just a single lateral scan in the x -direction is performed with the adaptive prism. As a first step, the actuation voltages of the adaptive elements are tuned as follows: the voltage of the adaptive lens U is kept constant at -40 V, while the whole voltage range of the adaptive prism is tuned, resulting in a lateral scan at constant axial position. The voltage U_1 on the adaptive prism is driven from -50 V to $+150$ V and the decreasing voltage of the adaptive prism U_2 is from $+150$ V to -50 V. Then, U increased by 10 V and again U_1 and U_2 are driven over the whole voltage range, until the static voltage U is tuned over the whole range. For each voltage pair,

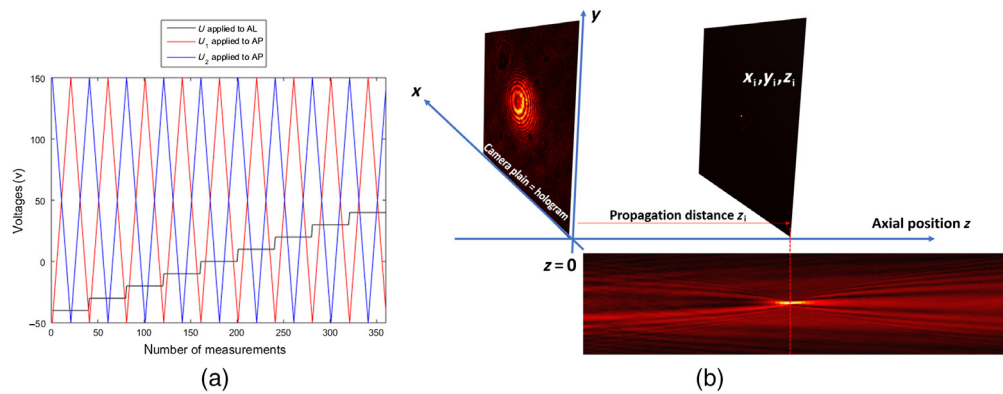


Fig. 6 (a) Voltage trajectories for the actuation of the adaptive elements for characterization. (b) Digital holographic propagation enables to determine the 3D focus position.

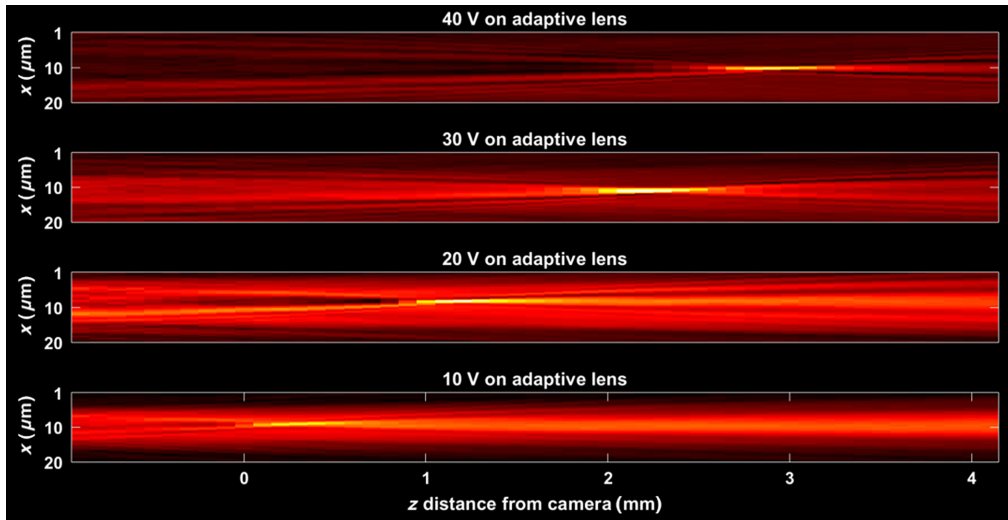


Fig. 7 Exemplary cross-section across amplitude reconstructions for different propagation distances at a constant lateral position.

a digital holographic measurement is performed, resulting in 360 measurements in total in this experiment.

Figure 7 shows cross-sections of the amplitude reconstructions for different propagation distances at different voltages.

The trajectory of lateral scanning is shown in Fig. 8. For each hologram, the propagation is performed, resulting in a cross-section amplitude image for each voltage configuration. The example in the figure shows the superposition of all reconstructions for scanned voltages on the adaptive prism, and for a constant axial position, at a voltage of 40 V on the adaptive lens.

The resulting scanned 3D area is shown in Fig. 9. The overall axial scan-range in this configuration is approximately 10.8 mm.

It is noteworthy that the z distance is measured relative to the camera position. The lateral scanning range amounts from -3.47 to $+3.47$ mm when $U_{AL} = -40$ V, from -2.67 to $+2.67$ mm when $U_{AL} = 0$ V, and from -2.31 to $+2.33$ mm when $U_{AL} = +40$ V, respectively. The results are consistent with analytical geometric considerations.

Using simple trigonometric calculations, the effective lateral scan angle can be determined and is displayed in Fig. 10(a). The standard deviation of the lateral tilt angles along each voltage

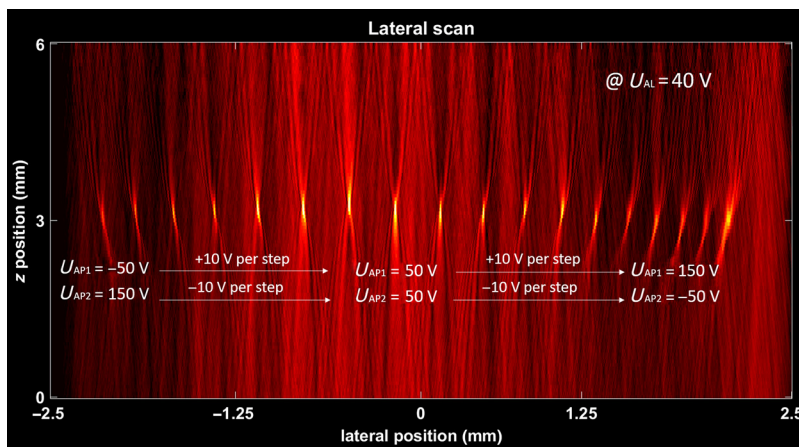


Fig. 8 Superposition of reconstructed amplitudes at different propagation distances. The voltage on the lens is kept fixed at $U_{AL} = 40$ V. Lateral scanning of the focus is accomplished by tuning the voltage on the adaptive prism.

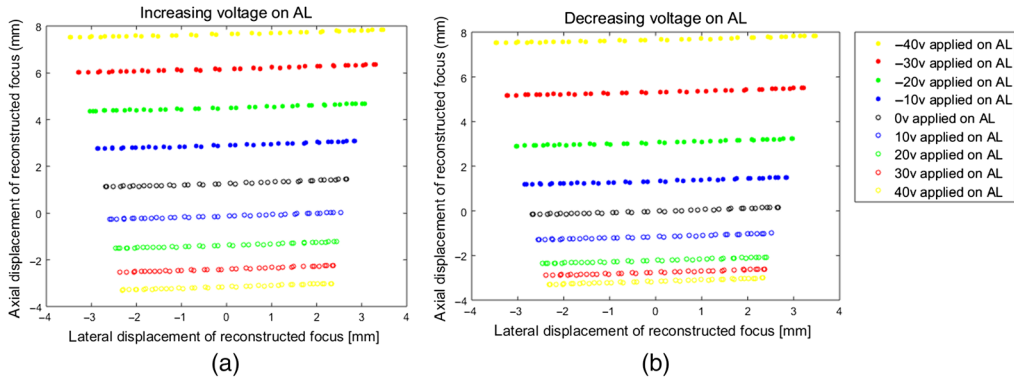


Fig. 9 The axial scanning and lateral scanning position of each focal spot in characterization setup. Hysteresis effects are clearly visible, when the color-coded scan lines are compared for increasing and decreasing voltages on the adaptive lens. (a) Increasing voltage on AL and (b) decreasing voltage on AL.

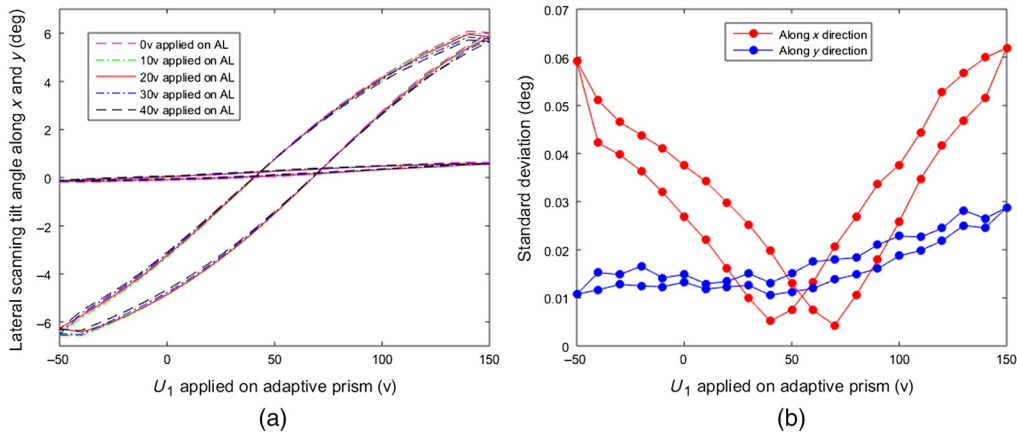


Fig. 10 (a) The induced wavefront tilt angles in the experiment at different axial positions. (b) The standard deviation of the lateral tilt angles along each voltage pair.

pair is shown in Fig. 10(b), the maximum standard deviation appears for the maximum angles and amounts to 1%, while for small angles, the standard deviation appears to be 0.05%.

For large tilt-angles of the adaptive prism, the focus quality and the peak intensity degrade due to aberrations. The by far greatest contribution to the aberrations, induced by tuning of the adaptive elements, is astigmatism. As in these experiments the scan lens has a comparably low refractive power, the spherical aberrations have a small effect in this configuration. Images of the resulting point-spread functions are shown in Fig. 11(a). The change of the astigmatism of the whole system during scanning is shown in Fig. 11(b). All other aberrations do not show significant contributions. Due to hysteresis, the axial displacements of the focal spot behave differently for decreasing and increasing voltages.

4 Experimental Validation

For the final all-adaptive scanning microscope, a 40× Olympus microscope objective (effective focal length = 4.5 mm, NA = 0.65) is employed as a scanning lens to further increase the NA and magnification of the system. The resulting axial scan range is reduced to around 500 μm. Laterally, the usable scan range amounts to approximately 130 μm. The theoretical axial and lateral resolutions of the system are 2.5 μm and 500 nm, respectively.

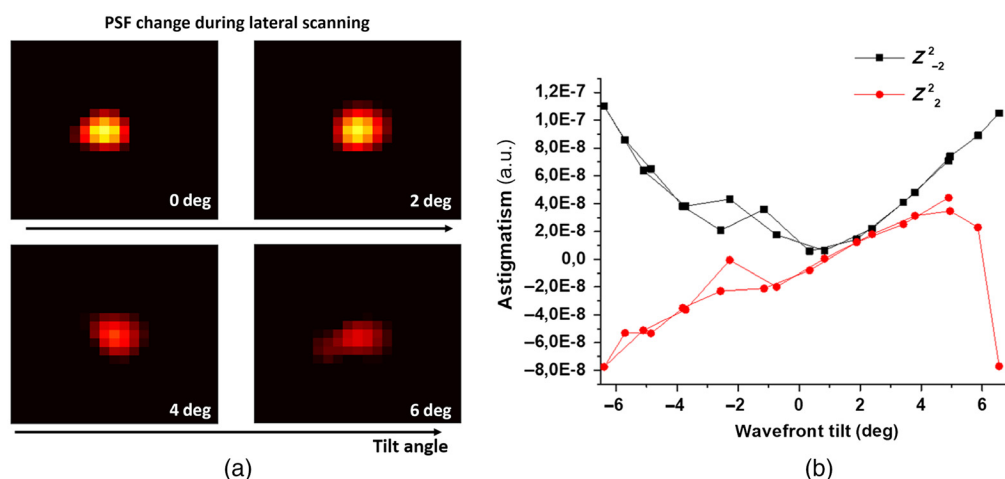


Fig. 11 (a) The left part of the figure shows the point-spread function at different lateral locations. The focus quality degrades during the lateral scanning. (b) This is mainly due to astigmatism.

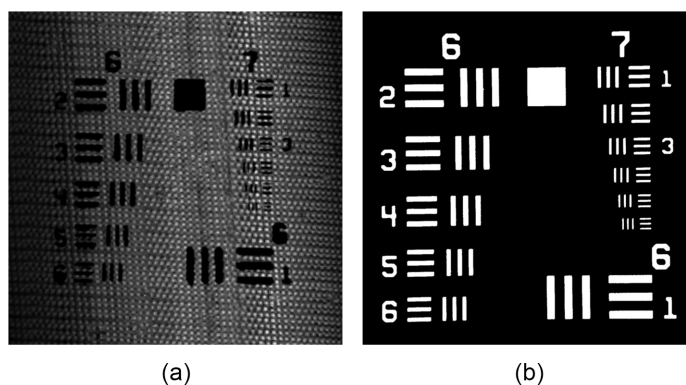


Fig. 12 A USAF test chart (b) was scanned pointwise by tuning of the adaptive prism. The superposition of the individual raster scanned images is shown in (b).

As a first step in the experiment, a USAF resolution test chart (Thorlabs R1DS1P) is used as a target. The all-adaptive scanning setup is applied in transmission geometry in a comparable way as shown in the characterization setup. Only the scanning lens is replaced by the above-mentioned microscope objective. The sample plane is imaged to a digital camera by a lens system. Without any voltage on the adaptive optical elements, the microscope objective creates a focus on the sample. By applying voltage trajectories on the adaptive prism, a lateral scanning is accomplished resulting in a shifting focus on the camera. For each voltage constellation, an image is acquired. By superposition of the individual single-focus images, the image of the USAF test target is obtained, as displayed in Fig. 12. The smallest elements (element 6 of group 7) of our USAF test chart is clearly resolved, which corresponds to a lateral resolution of $2.2 \mu\text{m}$. A slight tilt of the scans is observable, which is induced by a slightly rotated mounting of the adaptive prism, the optical setup, and camera.

4.1 3D Scanning of the Fluorescence of a Thyroid in Transgenic Zebrafish Embryos

The setup we used for the first all-adaptive 3D scanning experiments is shown in Fig. 13. The setup is used in reflection geometry. An LED is used for flood-illumination during alignment of the setup. The laser beam is scanned across the sample in three dimensions by just changing the voltages on the adaptive elements. The fluorescence is excited within the thyroid of a transgenic

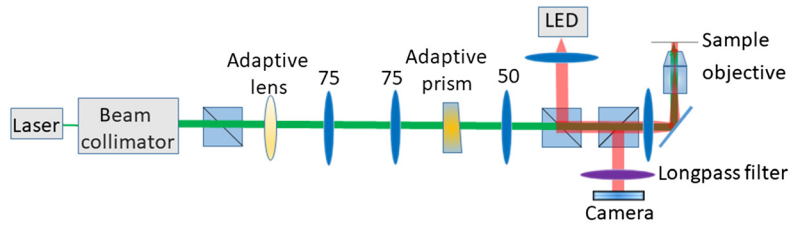


Fig. 13 3D scanning setup. An objective lens (40 \times , NA = 0.65) is used as a scanning lens. The LED is used for flood-illumination during alignment of the setup. The laser beam is scanned across the sample in three dimensions by just changing the voltages on the adaptive elements.

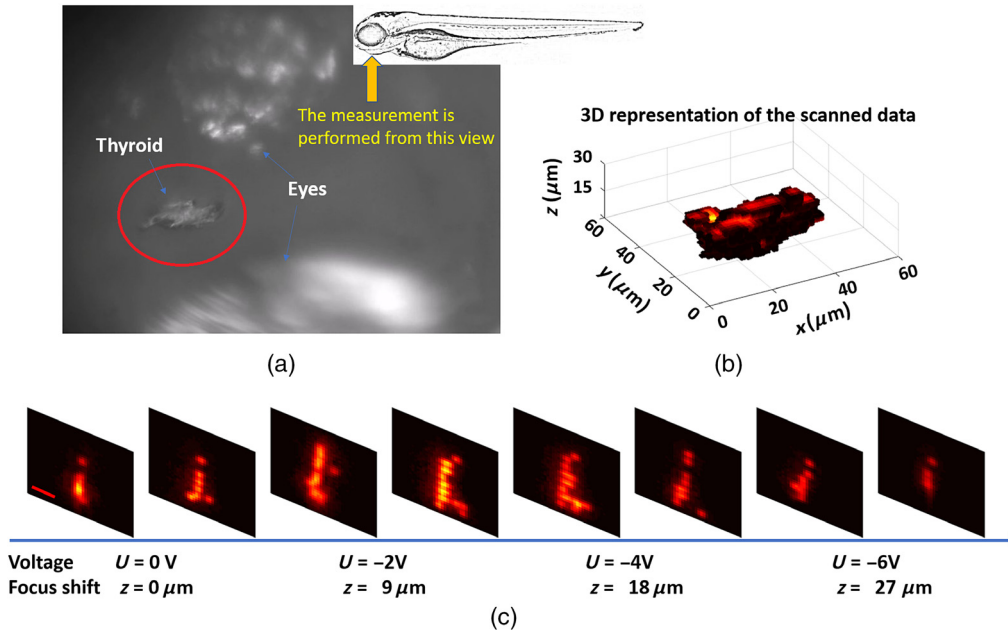


Fig. 14 (a) Dorsal view of the thyroid in the zebrafish embryo. The thyroid is located between the eyes, approximately 200 μm below the surface. (b) 3D scanning of the excited fluorescence of zebrafish. (c) Excited fluorescence of transgenic zebrafish embryo along different voltage pairs. Red scale bar is 20 μm .

zebrafish larvae. A long-pass filter in front of the camera in the detection path separates the fluorescence signal from the excitation. For each voltage combination, an image is recorded with the digital camera. As described earlier, the lateral scan is performed for a constant voltage on the adaptive lens. Then, the adaptive lens is tuned and the lateral scan is repeated for a different axial position. These individual scans are shown in Fig. 14(c). After scanning is completed, the data can be superimposed to the 3D view shown in the upper right of the figure. For future experiments, the setup is to be realized in a confocal geometry to reduce the out-of-focus signals by optical sectioning. Additionally, the detection geometry has to be adjusted, to keep the detection focused at the excitation, as currently tuning of the adaptive elements leads to a slight detuning of the setup.

5 Discussion

We demonstrate first all-adaptive 3D scanning, combining two adaptive scanning elements. This configuration has high potential to enable a compact and cost-effective in-line laser scanning microscope, without beam folding. The advantages of our approach in comparison to scanning using a spatial light modulator (SLM) are the large tuning range and the potentially high tuning

speed. Additionally, the refractive elements have a higher efficiency than the diffractive SLM versions. These advantages promise faster measurements in the sub-ms range and are thus important for fluorescence microscopy as they may result in a reduced exposure of the sample, minimizing bleaching effects. In the final microscope, the focus size in lateral dimension is approximately $1\ \mu\text{m}$. The scan range in air amounts to approximately $X = Y = 130\ \mu\text{m}$ in lateral direction and about $Z = 500\ \mu\text{m}$ in axial direction. However, there is still room for improvement. While the lateral full-width half maximum point-spread function-size of the system is below $2\ \mu\text{m}$ over the whole tuning range, the axial resolution is in the range of $10\ \mu\text{m}$. This could be improved by changing the setup to a confocal alignment. The precise control and orchestration of the adaptive elements is highly demanding, requiring either closed-loop iterations or system monitoring, e.g., using wavefront sensing techniques.¹² To ensure a high resolution in all-dimensions during scanning and to reduce the astigmatism, a multi-segmented lens is required to enable non-symmetric tuning. This further increases the difficulty for a precise control. Nevertheless, the presented approach has a high potential to improve the performance and increase the scanning flexibility for all point-scanning-based microscopy systems, paving the way to smart, computational microscopes.

Acknowledgments

The authors thank Moritz Stuermer for providing the adaptive lens and Pascal M. Weber for support in fabrication and testing of the adaptive prisms. This research was partially funded by German Research Foundation under Project Nos. CZ 55/32-2 and WA 1657/6-2 and by the China Scholarship Council under Project No. 201706500012. The authors declare no conflicts of interest.

References

1. M. Teich et al., "Adaptive particle image velocimetry based on sharpness metrics," *J. Eur. Opt. Soc.* **14**(1), 1–8 (2018).
2. K. Philipp et al., "Diffraction-limited axial scanning in thick biological tissue with an aberration-correcting adaptive lens," *Sci. Rep.* **9**(1), 1–11 (2019).
3. E. Scharf et al., "Video-rate lensless endoscope with self-calibration using wavefront shaping," *Opt. Lett.* **45**(13), 3629–3632 (2020).
4. S. W. Paddock, "Principles and practices of laser scanning confocal microscopy," *Mol. Biotechnol.* **16**(2), 127–149 (2000).
5. J. B. De Monvel, S. Le Calvez, and M. Ulfendahl, "Image restoration for confocal microscopy: improving the limits of deconvolution, with application to the visualization of the mammalian hearing organ," *Biophys. J.* **80**(5), 2455–2470 (2001).
6. Y. Chen et al., "High-resolution line-scanning optical coherence microscopy," *Opt. Lett.* **32**(14), 1971–1973 (2007).
7. A. D. Aguirre and J. G. Fujimoto, "Optical coherence microscopy," in *Optical Coherence Tomography*, W. Drexler and J. Fujimoto, Eds., pp. 505–542, Springer, Cham (2008).
8. A. Dixon, S. Damaskinos, and M. Atkinson, "Transmission and double-reflection scanning stage confocal microscope," *Scanning* **13**(4), 299–306 (1991).
9. J. Benschop and G. Van Rosmalen, "Confocal compact scanning optical microscope based on compact disc technology," *Appl. Opt.* **30**(10), 1179–1184 (1991).
10. N. Callamaras and I. Parker, "Construction of a confocal microscope for real-time xy and xz imaging," *Cell Calcium* **26**(6), 271–279 (1999).
11. H. Oku, K. Hashimoto, and M. Ishikawa, "Variable-focus lens with 1-kHz bandwidth," *Opt. Express* **12**(10), 2138–2149 (2004).
12. W. Wang et al., "Real-time monitoring of adaptive lenses with high tuning range and multiple degrees of freedom," *Opt. Lett.* **45**(2), 272–275 (2020).
13. N. Koukourakis et al., "Axial scanning in confocal microscopy employing adaptive lenses (CAL)," *Opt. Express* **22**(5), 6025–6039 (2014).
14. B. F. Grewe et al., "Fast two-layer two-photon imaging of neuronal cell populations using an electrically tunable lens," *Biomed Opt. Express* **2**(7), 2035–2046 (2011).

15. S. Piazza et al., “Enhanced volumetric imaging in 2-photon microscopy via acoustic lens beam shaping,” *J. Biophotonics* **11**(2), e201700050 (2018).
16. F. O. Fahrbach et al., “Rapid 3D light-sheet microscopy with a tunable lens,” *Opt. Express* **21**(18), 21010–21026 (2013).
17. M. Duocastella et al., “Fast inertia-free volumetric light-sheet microscope,” *ACS Photonics* **4**(7), 1797–1804 (2017).
18. R. M. Power and J. Huisken, “A guide to light-sheet fluorescence microscopy for multiscale imaging,” *Nat. Methods* **14**(4), 360–373 (2017).
19. K. Philipp et al., “Volumetric light-sheet microscopy employing an electrically tunable lens,” *Opt. Express* **24**(13), 15029–15041 (2016).
20. T. Hinsdale et al., “Volumetric structured illumination microscopy enabled by a tunable-focus lens,” *Opt. Lett.* **40**(21), 4943–4946 (2015).
21. M. Martí et al., “Fast axial-scanning widefield microscopy with constant magnification and resolution,” *J. Disp. Technol.* **11**(11), 913–920 (2015).
22. Y. Nakai et al., “High-speed microscopy with an electrically tunable lens to image the dynamics of *in vivo* molecular complexes,” *Rev. Sci. Instrum.* **86**(1), 013707 (2015).
23. A. J. Nichols and C. L. Evans, “Video-rate scanning confocal microscopy and microendoscopy,” *J. Vis. Exp.* (56), e3252 (2011).
24. S. Terrab et al., “Adaptive electrowetting lens-prism element,” *Opt. Express* **23**(20), 25838–25845 (2015).
25. O. D. Supekar et al., “Two-photon laser scanning microscopy with electrowetting-based prism scanning,” *Biomed Opt. Express* **8**(12), 5412–5426 (2017).
26. J. Lee, J. Lee, and Y. H. Won, “Image stitching using an electrowetting-based liquid prism with a fabrication method,” *Opt. Express* **29**(2), 729–739 (2021).
27. F. Lemke et al., “Piezo-actuated adaptive prisms for continuously adjustable bi-axial scanning,” *Smart Mater. Struct.* **29**, 095004 (2020).
28. F. Lemke et al., “Multiphysics simulation of the spherical deformation of piezo-glass membrane lenses including hysteresis, fabrication and nonlinear effects,” *Smart Mater. Struct.* **28**(5), 055024 (2019).
29. K. Philipp and J. Czarske, “Axial scanning employing tunable lenses: Fourier optics based system design,” *OSA Continuum* **2**(4), 1318–1327 (2019).
30. N. Koukourakis et al., “Photorefractive two-wave mixing for image amplification in digital holography,” *Opt. Express* **19**(22), 22004 (2011).

Wenjie Wang is a PhD candidate with the Laboratory for Measurement and Sensor System Techniques since November 2017. She was awarded the Chinese Scholarship Council scholarship for four years. Her research interests include the development and application of adaptive lenses and adaptive prisms, 3D scanning microscopy, and quantitative phase imaging.

Florian Lemke received his master’s degree in microsystems engineering from the University of Freiburg, Germany, in 2014. At the chair of Microactuators, he subsequently conducted research on piezo-controlled aberration-correcting lenses and adaptive prisms as part of his doctoral thesis, which he successfully completed in 2021. He was awarded with the “Best Student Award” for his work on prisms at the International Symposium on Optomechatronic Technology 2018.

Matthias C. Wapler studied physics at Imperial College London and completed his PhD in theoretical physics at the University of Waterloo and the Perimeter Institute and holds a post-doctoral position at the Center for Quantum Spacetime of Sogang University, Korea. He then changed his field into microsystems engineering at the University of Freiburg. There he currently works as a group leader and researcher with main interests in piezo- and micro-actuators, adaptive optics, and biomedical applications.

Ulrike Wallrabe studied physics at Karlsruhe University (today KIT), Germany. In 1992, she received her PhD for mechanical engineering on microturbines and micromotors. From 1989 to 2003, she was with Forschungszentrum Karlsruhe (today KIT) working on optical MEMS. Since 2003, she holds a professorship for microactuators in the Department of Microsystems

Engineering, IMTEK, at the University of Freiburg, Germany. Her focus lies in magnetic microsystems and in adaptive optics using piezo-actuators for tuning.

Jürgen W. Czarske is a professor and a director. He studied electrical engineering and physics and obtained his PhD and the Venia Legendi from Leibniz University. He has held visiting positions at NTT, MIT, Bell Labs, Stanford, Virginia Tech, NASA, and CalTech. His awards include 1996 AHMT Prize, 2008 Berthold Leibinger Innovation Prize, 2019 OSA Joseph Fraunhofer Award/Robert M. Burley Prize, and the Laser Instrumentation Award of IEEE Photonics Society. He is a fellow of OSA, SPIE, and EOS.

Nektarios Koukourakis studied electrical engineering at Ruhr-University, Bochum, where he also received his PhD in 2012. Since 2013, he has been a research fellow at TU Dresden where he became head of the biophotonics group in 2016. Since 2020, he also has been a chief technology officer at the competence center BIOLAS. His current research interests include quantitative phase imaging, holography, wavefront shaping, computational and adaptive microscopy, lensless endoscopy, and fiber-based optical communication.